Research Article | Vol. 29, No. 26 / 20 Dec 2021 / *Optics Express* 43464

Optics EXPRESS

Design method for a reflective optical system with low tilt error sensitivity

ZICHANG QIN,[1,2,3] XIAODONG WANG,[1,2] CHENGMING REN,[1,3] YUNSHENG QI,[1,3] AND QINGYU MENG[1,*]

[1] *Changchun Institute of Optics, Fine Mechanics and Physics, Chinese Academy of Sciences, Jilin, Changchun 130033, China*
[2] *CAS Key Laboratory of On-orbit Manufacturing and Integration for Space Optics System, Changchun Institute of Optics, Fine Mechanics and Physics, Chinese Academy of Sciences, Jilin, Changchun 130033, China*
[3] *University of the Chinese Academy of Sciences, Beijing 100049, China*
[*] *mengqy@ciomp.ac.cn*

Abstract: The realization of the final performance of the optical system depends not only on the aberration correction of the optical design but more importantly on the control of the position error of the optical element during the construction process. Therefore, reducing the error sensitivity of the optical system is an important part of the optical system design process. In order to obtain an optical system with low error sensitivity, this paper proposes an evaluation function of the tilt error sensitivity of the optical system and establishes a desensitization design method for the optical system. Taking an off-axis three-mirror optical system as an example for desensitization design. By comparing the variation of wave front error (WFE) caused by the tilt error of the optical system before and after the desensitization design, the correctness of the evaluation function and the effectiveness of the desensitization design method of the optical system are proved.

1. Introduction

Error sensitivity can reflect the degradation of image performance after misalignment of optical system. Optical systems with low error sensitivity have looser tolerance requirements, which can better reduce the difficulty of optical system processing and assembly as well as reduce optical system manufacturing costs, making the system more feasible.

As an important classification of optical system types, reflective optical systems have many applications or plans in advanced optical systems, including a large number of coaxial reflective optical systems such as ground-based optical telescopes [1–3], Hubble Telescope [4], James Webb Space Telescope [5], and off-axis reflective optical systems, such as "Tianwen-1" High Resolution Imaging Camera (HiRIC) [6], free-form imaging systems [7–9], large space telescope [10–12]. With the continuous improvement of application requirements, reflective optical systems are developing in the direction of large aperture, long focal length, large field of view (FOV), and surface complexity, and the corresponding error sensitivity and manufacturing cost have become higher and higher. Therefore, the theoretical research on the influence of optical system parameters on the error sensitivity of optical system and the establishment of the design method of reflective optical system with low error sensitivity are helpful to reduce the difficulty and cost of optical system construction, which is of great significance to the development of optical instruments.

In order to obtain the optical system with low error sensitivity, in the absence of error sensitivity theory and desensitization design method, it is often necessary to carry out the optimal design of a large number of samples, analyze the tolerance of a large number of optimization results, and select the design results with low error sensitivity. This design process is not only inefficient, but

#447556 https://doi.org/10.1364/OE.447556
Journal © 2021 Received 4 Nov 2021; revised 28 Nov 2021; accepted 29 Nov 2021; published 13 Dec 2021

also blind. In order to effectively obtain optical systems with low error sensitivity, researchers have proposed and established a variety of error sensitivity evaluation functions from different perspectives and carried out research on optical system desensitization design methods. The more typical method at the beginning of the research is the global optimization method [13], in which the system with good tolerance robustness is selected from a large number of design samples to obtain an optical system with low error sensitivity by using the traditional large-sample optimization-iterative method. With the improvement of the understanding of error sensitivity, optical designers have gradually shifted their research focus to the control of key parameters in optical systems, and the representative methods are: " Adjustment-Optimization-Evaluation" (AOE) desensitization design process [14], "θ-segmentation" method [15,16], the multiple structure method [17], and the method to control the aspheric surface parameters [18] and so on. Other scholars found that some aberrations of optical systems have a large impact on the error sensitivity, and accordingly proposed the method of adding aberration control factors in the optimization process [19,20]. In recent years, with the continuous improvement of the design index of optical systems, more and more design methods for optical systems with free-form surface are proposed [21–25], and some scholars found that the application of free-form surface can reduce the error sensitivity of optical systems [26–29].

Tilt is a representative form of error (misalignment) in the optical system. If the optical path difference (*OPD*) is used as the image performance evaluation criterion, when the optical system with low error sensitivity is interrupted by the error, and the variation of *OPD* is small. In this paper, the relationship between the *OPD* variation due to the tilt error of the optical system and the parameters of the optical system is studied theoretically based on the geometric optics method. The tangent slope at the intersection of the ray and mirror is identified as the key factor to characterize the error sensitivity of the optical system, and the tilt error sensitivity evaluation function *S* with the tangent slope as the core is proposed. A comprehensive reflective optical system design method with low tilt error sensitivity is established. The method takes into account the uniformity of the error sensitivity of each mirror of the system while optimizing the imaging performance of the system and controlling the tilt error sensitivity of the optical system. By introducing the standard deviation of the error sensitivity in the evaluation function, the error sensitivity of one mirror in the design scheme is avoided to be too high.

In order to verify the correctness of the theoretical research results and the effectiveness of the desensitization design method, an off-axis three-mirror optical system with a focal length of 100 mm, an *F*-number of 5, and an FOV of 1°×1° was used as an example to design an optical system with low tilt error sensitivity. The correctness and validity of this paper were verified by comparing the variation of WFE due to tilt error of the optical system before and after the desensitization design.

2. Theoretical analysis of tilt error sensitivity

OPD is a common criterion for evaluating the imaging performance of an optical system in geometric optics. This section applies the method of ray tracing to analyze the mathematical relationship between the variation of *OPD* and the parameters of the optical system when the optical system is interrupted by tilt error, and then proposes an evaluation function for sensitivity to tilt error.

2.1. Mathematical model of the single-mirror optical system

First, a mathematical model of single-mirror reflective optical system is established, as shown in Fig. 1. In the figure, the *Z*-axis is the optical axis, and the incidence ray propagates in the direction of the optical axis. *PM* and *PM'* are the original position state of the mirror and the position state with the tilt error. Point *O* is the intersection point of the mirror and the optical axis, and the *IMP* is the image plane. The distance from the image plane to the point *O* is *L*. In order to simplify the understanding, the mirror surface adopts the common conic surface, and the form is as follows:

$$z = \frac{cr^2}{1 + \sqrt{1 - (1 + k)c^2 r^2}}, \tag{1}$$

where z is the sag of the surface parallel to the optical axis, c is the curvature of the surface, k is the quadric constant and r is the radial distance.

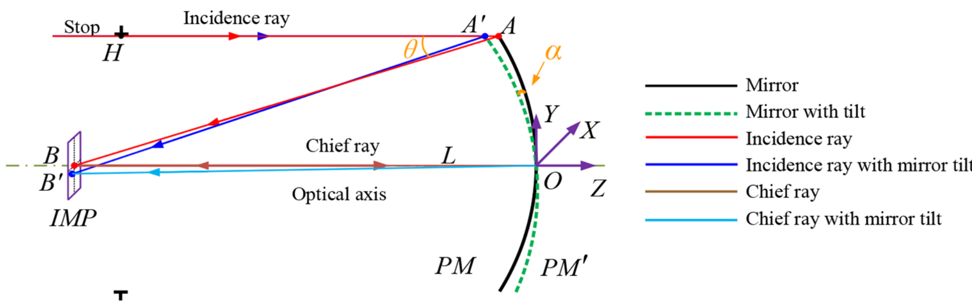

Fig. 1. Mathematical model of single-mirror optical system

The tilt error of the mirror is often two-dimensional, and any tilt error can be decomposed into two directions. In order to facilitate analysis, we make a coordinate transformation. The V coordinate axis is established according to the comprehensive tilt direction, as shown in Fig. 2(c). When the mirror tilts, a comprehensive oblique plane is selected for analysis. The tilt error diagram of the mirror is shown in Fig. 2. The black ellipse outline represents the original state of the mirror, while the red shaded line area in Fig. 2(a) represents the mirror with tilt error in the sagittal direction, and the sagittal tilt error angle is ρ; the blue shaded line in Fig. 2(b) represents the mirror with the tilt error in the tangential direction, and the tangential tilt error angle is μ; the green shaded line in Fig. 2(c) represents the mirror with the integrated tilt, and the integrated tilt error angle is α.

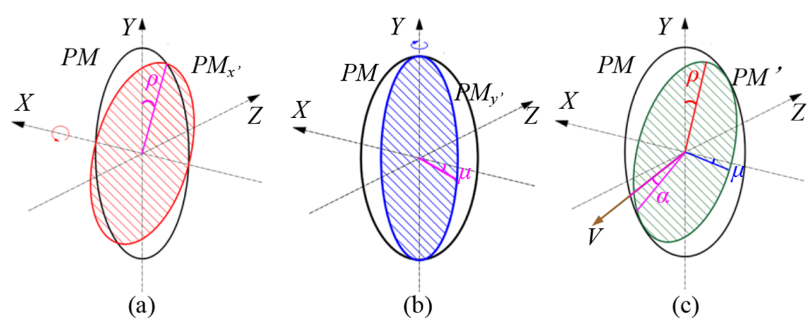

Fig. 2. Mirror tilt error diagram. (a) Mirror with sagittal tilt, (b) Mirror with tangential tilt, (c) Mirror with integrated tilt

The up ray of the tilted oblique section is selected as the characteristic ray for analysis. Before the tilt error generated, the intersection of the incidence ray with the mirror and the IMP is A, B, respectively, and the OPD of the characteristic ray is:

$$OPD = HA + AB - (BO + OB). \tag{2}$$

Optics EXPRESS

After the tilt error generated, the intersection of the incidence ray with the mirror and the *IMP* is *A'*, *B'*, respectively, and the *OPD'* of the characteristic ray is:

$$OPD' = HA' + A'B' - (BO + OB'). \tag{3}$$

The variation of *OPD* is as Eq. (4), we divide the variation of the *OPD* into three parts for analysis, namely: Part I, Part II, Part III:

$$\begin{aligned}\Delta OPD &= OPD - OPD' \\ &= \underbrace{AA'}_{\text{Part I}} + \underbrace{AB - A'B'}_{\text{Part II}} + \underbrace{OB' - OB}_{\text{Part III}}.\end{aligned} \tag{4}$$

As for Part I, Fig. 3 is a simplified diagram of Part I. Make a perpendicular to the extended line of incidence ray through point O and intersect at point C, where α is the tilt error angle, β is the angle between OA and OC, the height of the incidence ray is h. Part I is derived from the geometric relationship:

$$\begin{aligned}AA' &= A'C - AC \\ &= h\tan(\alpha+\beta) - h\tan\beta \\ &\approx h\tan\alpha.\end{aligned} \tag{5}$$

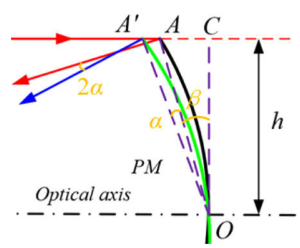

Fig. 3. Part I of ΔOPD

The analysis of Part I shows that the variation of *AA'* is only related to the tilt error angle α.

In order to give the mathematical relationship concisely, so that let the mirror surface be a paraboloid, that is, k= -1. Use point O as the origin to establish a Cartesian coordinate system. The direction of the optical axis is the positive direction of the Z axis, and the upward direction of the origin is the positive direction of the V axis. The mirror equation can be expressed as:

$$v = \sqrt{\frac{2z}{c}}(z<0). \tag{6}$$

The coordinates of point A can be obtained as $A(-\frac{1}{2}ch^2, h)$, and the coordinates of point *A'* is $A'(-\frac{1}{2}ch^2 - h\tan\alpha, h)$. Based on this, *A'H* can be calculated as:

$$A'H = L - \frac{1}{2}ch^2 - h\tan\alpha. \tag{7}$$

According to the trigonometric function relationship, *AB* and *A'B'* are calculated as:

$$AB = \frac{AH}{\cos 2\theta}. \tag{8}$$

$$A'B' = \frac{A'H}{\cos 2(\theta+\alpha)}. \tag{9}$$

Optics EXPRESS

The difference between Eq. (9) and Eq. (8) is Part II:

$$AB - A'B' = W[\frac{1}{\cos 2\theta} - \frac{1}{\cos 2(\theta+\alpha)}] + \frac{h\tan\alpha}{\cos 2(\theta+\alpha)}, \tag{10}$$

where $W = L - \frac{1}{2}ch$,set:

$$T(\theta) = \frac{1}{\cos 2\theta} - \frac{1}{\cos 2(\theta+\alpha)}. \tag{11}$$

$$t(\theta) = \frac{1}{\cos 2\theta}. \tag{12}$$

The first derivative and second derivative of $t(\theta)$ are shown in Eq. (13) and Eq. (14) respectively:

$$t'(\theta) = \frac{2\sin 2\theta}{\cos^2 2\theta}, \tag{13}$$

$$t''(\theta) = \frac{4(\cos^3 2\theta + 2\cos 2\theta \sin^2 2\theta)}{\cos^4\theta}. \tag{14}$$

When $\theta \in (0, \pi/2)$, both $t'(\theta)$ and $t''(\theta)$ are always greater than zero. Explain that within this range, $T(\theta)$ is a monotonically increasing function and the growth rate is getting faster and faster. The latter part of Eq. (10) increases with the increase of θ. Therefore, as θ increases, $t(\theta)$ increases, $T(\theta)$ increases, and ΔOPD increases.

Part III can be expressed as:

$$\begin{aligned} OB' - OB &= OB(\tfrac{1}{\cos 2\alpha} - 1) \\ &= L(\tfrac{1}{\arctan^2\alpha - 1}). \end{aligned} \tag{15}$$

It can be seen that Part III is only related to L and α, and not to θ.

Through the analysis of the three parts, the variation rule of ΔOPD is as follows: when the tilt error angle α is constant, ΔOPD increases with the increase of the incidence angle. When the design index of the optical system is fixed, the incidence direction of the ray cannot be changed. The reflection direction of the ray can be changed by changing the parameters of the mirror during the design process.

2.2. Mathematical model of the two-mirror optical system

The analysis method of the single-mirror optical system is extended to the two-mirror optical system, and the two-mirror optical system adopts Cassegrain form with conic surface type. The calculation method of the two-mirror optical system is similar to that of single-mirror optical system, and only the key derivation steps and main conclusions are given here.

The schematic diagram of the two-mirror optical system is shown in Fig. 4. *PM* and *PM'* are the original position state of the mirror and the position state after the tilt error is generated. Point *O* is the intersection point between the primary mirror and the optical axis, *SM* represents the secondary mirror, *IMP* represents the image plane, and point *A*, *B*, and *C* are the intersection points of the incidence ray with the *PM*, *SM* and the *IMP*, respectively. Point *A'*, *B'*, and *C'* are the incidence ray and *PM'*, *SM* and the *IMP* after the tilt error. Make a vertical line passing through point *I* which is on the optical axis to intersect the incidence ray with point *H*, and the stop is set at point *H*. Point *G* and point *G'* are the intersection points of the chief ray and the *SM* before and after the tilt error, and the tilt error angle is α.

Optics EXPRESS

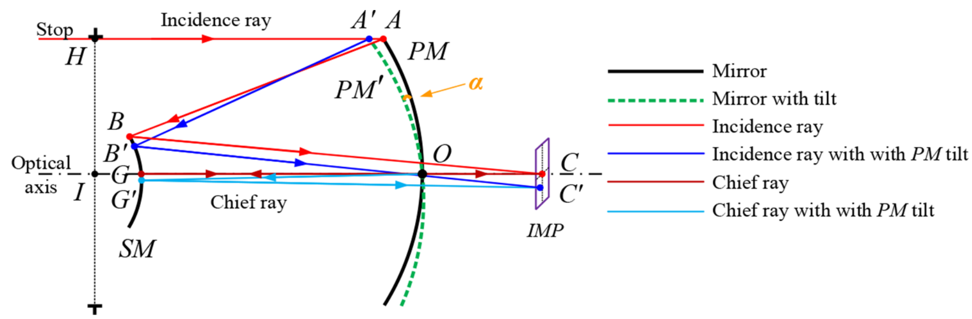

Fig. 4. Mathematical model of two-mirror optical system

Before the optical system tilted, the *OPD* of the incidence ray is:

$$OPD = OP_I - OP_C, \tag{16}$$

where the optical path of the incidence ray is OP_I, the optical path of the chief ray is OP_C, they are as follow:

$$OP_I = HA + AB + BC. \tag{17}$$

$$OP_C = IO + OG + GC. \tag{18}$$

After the optical system tilted, the *OPD'* of the incidence ray is:

$$OPD' = OP_I{}' - OP_C{}', \tag{19}$$

where the optical path after tilt of the incidence ray is OP_I*'*, and the optical path after tilt of the chief ray is OP_C*'*, they are as follows:

$$OP_I{}' = HA' + A'B' + B'C'. \tag{20}$$

$$OP_C{}' = IO + OG' + G'C'. \tag{21}$$

The variation of optical path difference ΔOPD is:

$$\begin{aligned}\Delta OPD &= OPD - OPD' \\ &= (OP_I - OP_C) - (OP_I{}' - OP_C{}') \\ &= \Delta OP_I + \Delta OP_C \\ &= \underbrace{HA - HA'}_{\text{Part I}} + \underbrace{AB + BC - A'B' - B'C'}_{\text{Part II}} + \underbrace{OG' + G'C - OG - GC}_{\text{Part III}}.\end{aligned} \tag{22}$$

The calculation method of Part I and Part III are the same as that in section 2.1, and they are only related to the tilt error angle α, so only Part II needs to be calculated. Here we want to prove how Part II changes when the incidence angle is increased as the tilt error angle is the same. The variation of *OPD* before the increase of incidence angle is expressed as the Eq. (22). When the incidence angle increases, the variation of *OPD* is expressed as:

$$\Delta OPD_{(\theta')} = OPD_{(\theta')} - OPD_{(\theta')}'. \tag{23}$$

In the Eq. (23), θ*'* is the increased incidence angle, and $OPD_{(\theta')}$ is the OPD of the incidence ray, $OPD_{(\theta')}$*'* is the OPD when the optical system tilted, respectively:

$$\begin{cases} OPD_{(\theta')} = OP_{I(\theta')} - OP_C \\ OPD_{(\theta')}' = OP_{I(\theta')}' - OP_C' \end{cases}, \tag{24}$$

where $OP_{I(\theta')}$*'* is the optical path of the incidence ray, $OP_{C(\theta')}$*'* is the optical path of the chief ray, Before and after the incidence angle increases, the difference of the variation of *OPD* when the system is tilted is as follows:

$$\Delta OPD(\theta) = OP_{I(\theta')} - OP_I - (OP_{I(\theta')}' - OP_I'). \tag{25}$$

Next, the method of analytic geometry is used to derive the relationship of rays. Pass the point *B'* to make the *AB* parallel line and intersect the ray extension line at the point *A''*, and pass the point *B'* to make the *BC* parallel line to intersect the *IMP* at the point *C"*, as shown in Fig. 5. Pass point *A* and make a perpendicular line to intersect point *A''B'* at point *T*. Pass point *B'* to make the *AB* perpendicular to point *AB* at point *D*. Pass point *B'* to make the *BC* perpendicular to point *BC* at point *J*. Pass point *B* to make *A''B'* perpendicular to intersect *A''B'* extension line at point *K*. The enlarged views in the green box in Fig. 5 are shown in Fig. 6. In Fig. 6, θ_1 is the incidence angle at the intersection of the ray and the *PM*, and θ_2 is the incidence angle at the intersection of the ray and the *SM*.

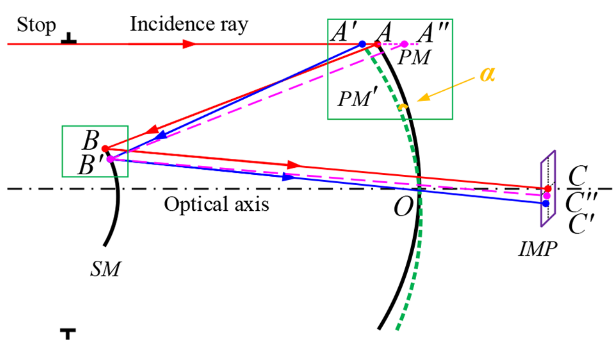

Fig. 5. Auxiliary line diagram of the two-mirror system

Find the relationship between the incidence angles θ_1, θ_2, the tilt error angle α and *BB'*. Assuming that the tilt angle α, angle θ_2 are constant, and angle θ_1 is a variable. The purpose is to show that when the incidence angle θ_1 increases, how *BB'* and ω change. Angle ω is the angle between *BB'* and *B'K*. It can be seen from Fig. 6(b) that when angle θ_1 increases, *BB'* and ω must increase.

The following equation can be obtained from the trigonometric relationship:

$$\begin{cases} BD = BB' \cos\omega \\ BJ = BB' \cos(\omega - 2\theta_2) \end{cases}. \tag{26}$$

$$AT = BK = BB' \sin\omega. \tag{27}$$

Optics EXPRESS

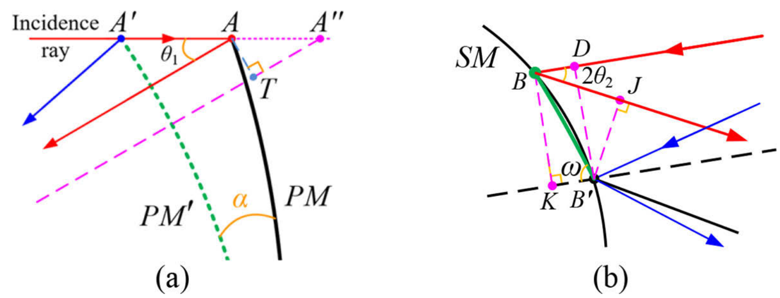

Fig. 6. Auxiliary line detail drawing (Enlarged view of the green box in Fig. 5). (a)Detail of the intersection of the ray and *PM*, (b) Detail of the intersection of the ray and *SM*

$$A''T = \frac{AT}{\tan 2\theta_1} = \frac{BK}{\tan 2\theta_1} = \frac{BB'\sin\omega}{\tan 2\theta_1}. \tag{28}$$

$$\begin{aligned} A'B' - B'T &= AT(\frac{1}{\sin 2\alpha} - \frac{1}{\tan 2\alpha}). \\ &= AT\tan\alpha \end{aligned} \tag{29}$$

We want to explain the change trend of $\Delta OPD(\theta)$ when *BB'* and ω increase. Here we calculate the absolute value of $\Delta OPD(\theta)$, avoiding the sign problem.

$$\begin{aligned} |\Delta OPD(\theta)| &= |(A'B' + B'C') - (AB + BC)| \\ &= \left| \begin{array}{l} (A'B' + B'T' + A''T - A''B' + B'C'' + B'C' - B'C'')- \\ (AD + BD + BJ + JC) \end{array} \right| \\ &= |(A'B' - B'T) - (BD + BJ)| \\ &= |AT\tan\alpha - (BD + BJ)|. \end{aligned} \tag{30}$$

Since the tilt error angle α is very small, $\tan\alpha \approx 0$, so Eq. (30) can be simplified as:

$$\begin{aligned} |\Delta OPD(\theta)| &= |AT\tan\alpha - (BD + BJ)| \\ &\approx |BD + BJ|. \end{aligned} \tag{31}$$

As shown in Fig. 7, points $D_{(\theta)}$, $B_{(\theta)}$, $J_{(\theta)}$ are the points on the ray when the system is tilted, and angle $\omega_{(\theta)}$ is the angle between *BB'* and *B'K* before the incidence angle increased. Points $D_{(\theta')}$, $B_{(\theta')}$, $J_{(\theta')}$ are the points on the ray, and angle $\omega_{(\theta')}$ is the angle between *BB'* and *B'K* when the system is tilted after the incidence angle increased. We have obtained in the previous derivation that the Part II of the ΔOPD is a monotonically increasing function and the growth rate is getting faster and faster [as given by Eqs. (13,14)], so we can know that after the incidence angle increases, with the same tilt error, the value of $BD + BJ$ is greater, and $|\Delta OPD(\theta)|$ is greater.

The analysis in sections 2.1 and 2.2 shows that the angle of incidence ray is the key factor affecting the error sensitivity of the mirror. The mathematical analysis methods applied in the single-mirror and the two-mirror mathematical model and the conclusions obtained are also applicable to the three-mirror and even multi-mirror reflective optical systems. Therefore, the mathematical derivation of the multi-mirror optical system will not be done here.

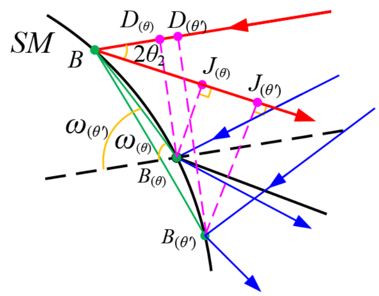

Fig. 7. Ray trace diagram before and after the angle θ_1 increases

3. Evaluation function and desensitization design method

Based on the analysis in Section 2, it is known that the system with large incidence angle has a larger variation of *OPD* and higher error sensitivity when interrupted by tilt error. Accordingly, we propose an optical system tilt error sensitivity evaluation function *S*, and establish an optical system desensitization design method.

3.1. Establishing the sensitivity evaluation function

According to the previous theoretical analysis, it is known that the tilt error sensitivity can be reduced by controlling the slope *K* of the mirror at the intersection of the ray and the mirror. According to the conclusion of the analysis, the greater the *K* is, the lower the tilt error sensitivity of the system is. However, it is difficult to set the upper threshold of *K*. We prefer to compare the error sensitivity by comparing the degree of the evaluation function close to zero. Therefore, we choose the absolute value τ of the slope of the normal at the intersection of the ray and the mirror as the evaluation function. The relationship between them is shown in Fig. 8. The blue dashed line and the black dashed line are the tangent and normal slope at the intersection of the ray and the mirror respectively, and the purple dashed line and the brown dashed line are the tangent and normal slope at the intersection of the ray and the mirror after generating the tilt error, which can be obtained from the trigonometric relationship as follows:

$$K = \tan\theta. \tag{32}$$

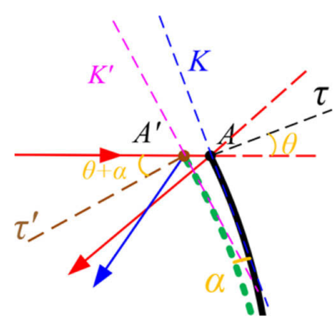

Fig. 8. Relation diagram of incidence angle and *K*

Optics EXPRESS

Define the tilt sensitivity evaluation function as S:

$$S = \frac{\sum_{m=1}^{M} \sqrt{\frac{\sum_{n=1}^{N} \tau_{n,m}^2}{n}}}{m}, \tag{33}$$

where $\tau = |1/k|$, n is the serial number of the mirror, m is the serial number of the FOV point, M is the quantity of the FOV point, and N is the quantity of the mirror.

Basis on these, considering the system as a whole, it is necessary to avoid the situation that the tilt error sensitivity of one mirror in the system is too high and the tilt error sensitivity of another mirror is too low, that is, the error sensitivity of the system cannot be uniformly distributed to each mirror. Therefore, the standard deviation is introduced to ensure a better uniformity of the error sensitivity of each mirror of the system.

The standard deviation of S is:

$$\sigma = \sqrt{\frac{1}{\mathrm{N}} \sum_{n=1}^{N} (S_n - \overline{S_n})^2}. \tag{34}$$

The comprehensive evaluation function Sen of tilt error sensitivity is defined as:

$$Sen = S \pm \sigma, \tag{35}$$

where the ± sign represents the fluctuation range of the error sensitivity of the optical system, and σ is the standard deviation of S. The smaller the range of the (S-σ, S+σ) interval is, the more uniformly the tilt error sensitivity of the optical system is considered to be distributed.

3.2. Establishing the desensitization design method

Based on the analysis in Section 2.1 and Section 2.2, a design method of reflective optical system with low tilt error sensitivity is proposed. The design process is shown in Fig. 9, which is mainly divided into four steps:

(1) Construct the initial system according to the requirements of the optical system index.

(2) Imaging performance optimization. In the optimization process, parameters such as thickness, radius, and conic are set as variables for optimization, while the structural sizes of the optical system are controlled. If the designed system is an off-axis system, ray obscuration is also avoided. After optimization, the image performance is judged, and the system that meets the image performance requirements enters the desensitization design step.

(3) Error sensitivity optimization. The error sensitivity of the optical system is evaluated, and the system that does not meet the judgment threshold of S is designed for desensitization, and the method for determining the judgment threshold is described in section 4.1. The core of the desensitization design process is to control the sensitivity evaluation function S to continuously reduce the error sensitivity of the optical system. Until the optical system meets the image performance requirements and sensitivity requirements at the same time, then the system is output.

(4) Error sensitivity uniformity optimization. If you want to avoid the situation where the sensitivity of some mirrors is too high and the sensitivity of some mirrors is very low in the optical system, a comprehensive optimization of the uniformity of error sensitivity can be carried out. The purpose is to make the optical system more evenly distribute the error

Optics EXPRESS

sensitivity of each mirror. The core of this method is to constrain the standard deviation of the S on the basis of controlling the error sensitivity. The image performance of the system that has completed the optimization of error sensitivity uniformity is evaluated. If the image performance is satisfied, the design can be output as the final result. If the image performance is unsatisfied, the comprehensive optimization of error sensitivity needs to be carried out again.

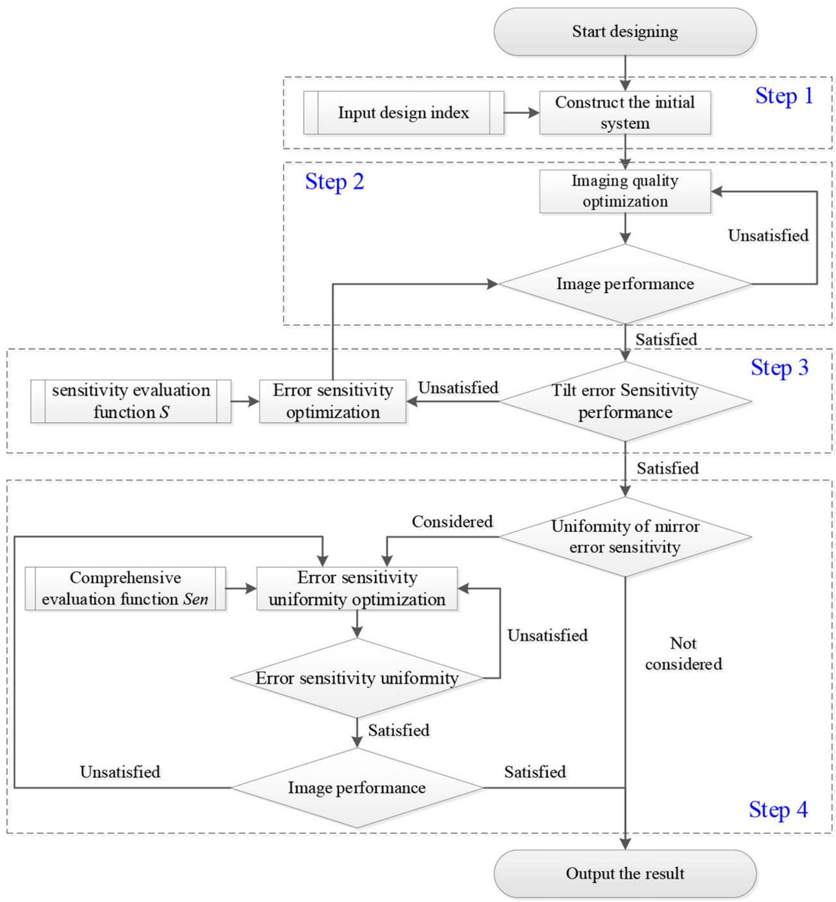

Fig. 9. Flow diagram of reflective optical system with low tilt error sensitivity

4. Desensitization design example and sensitivity analysis

In this section, an off-axis three-mirror optical system with a focal length of 100 mm, an F-number of 5, an FOV of $1°\times1°$, and an image performance evaluation wavelength of 550 nm is used as an example for desensitization design to verify the effectiveness of the desensitization design method.

4.1. Judgement threshold setting

S is the concept of tilt error sensitivity evaluation function that was proposed for the first time. The tilt error sensitivity judgement threshold is a S-centered threshold for judging whether an optical system satisfies low tilt error sensitivity. If the S of the optical system is less than the

Optics EXPRESS

threshold, the system is considered to meet the low error sensitivity requirement. However, for different types of optical systems, the error sensitivity judgment thresholds are different. For the optical system designed in this paper, since the optimal judgment threshold of *S* cannot be given directly yet, the initial judgment threshold is prepared to be determined by statistical analysis, and the initial judgment threshold is discussed and optimized after the design is completed.

In the validation design, to initially determine the threshold of *S*, 3000 groups of off-axis three-mirror optical system with the same index parameters were randomly generated within a certain range of structural parameters (*SM* to *PM* obscuration ratio (0.3, 0.5), *TM* to *SM* obscuration ratio (1.5, 1.8), and *SM* magnification (1.5, 1.8)). The distribution of their *S* is shown in Fig. 10. The statistics shows that the *S* of all 3000 groups of optical systems is greater than 0.085, and the *S* threshold is set to 0.085 in the desensitization design process.

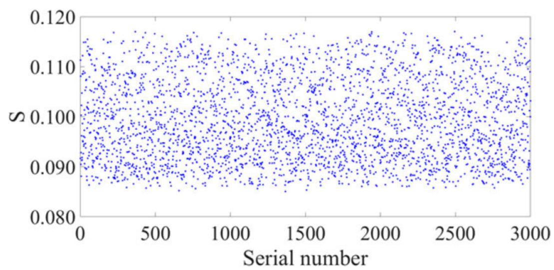

Fig. 10. *S* distribution diagram of 3000 groups of optical systems

The image performance threshold is set to a root-mean-square (RMS) WFE of 0.030λ±10%, that is, 0.0270λ~0.0330λ.

4.2. Design process

Applying the method of solving the third-order aberration, the initial structure of the coaxial three-mirror optical system (*SM* to *PM* obscuration ratio of 0.5, *TM* to *SM* obscuration ratio of 1.5, *SM* magnification of 1.5) is established, and the off-axis system is obtained through the FOV offset. The FOV of the off-axis optical system is -10°~-11° in the sagittal direction and -0.5°~0.5° in the tangential direction, and the secondary mirror is set as the aperture stop to form a Cook three-mirror optical system without relay image plane, named “system 0” as shown in Fig. 12(a).

The system after image performance optimization named “System 1” is shown in Fig. 12(b), and the RMS WFE of “System 1” is 0.0297λ. Through the analysis, the *S* of “System 1” is 0.197, but the tilt error sensitivity is high, so the desensitization design needs to be carried out. The *S* of the system was set as the optimization variable, and the *S* was continuously reduced through multiple optimizations to obtain “System 2”, “System 3”. . . "System 7” six systems in total. The layout of “System 7” is shown in Fig. 12(c). The RMS WFE of “System 7” is 0.0299λ and the *S* is 0.078. The imaging performance and error sensitivity both meet the requirements and can be output as the design result. Desensitization optimization process diagram is shown in Fig. 11.

Six systems, “System 8”, “System 9”. . . "System 13”, were obtained for this optimization. The layouts of “System 10”, “System 11” and “System 13” are shown in Fig. 12(d), Fig. 12(e) and Fig. 12(f). In the second stage of optimization, the image performance, the tilt error sensitivity evaluation function *S* and the standard deviation of the system are taken into consideration, and the image performance of “system 11” is good; the error sensitivity is low, and the standard deviation of the error sensitivity is minimal, which is the optimal system. The RMS WFE of “System 11” is shown in Fig. 12(g).

Optics EXPRESS

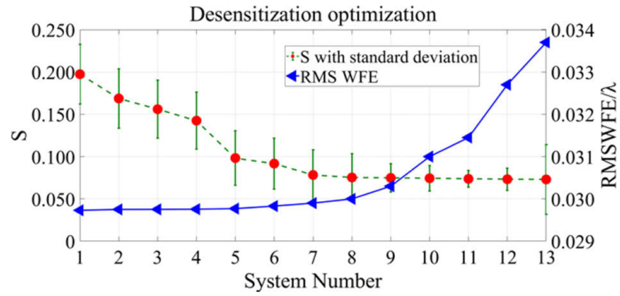

Fig. 11. Desensitization optimization process diagram

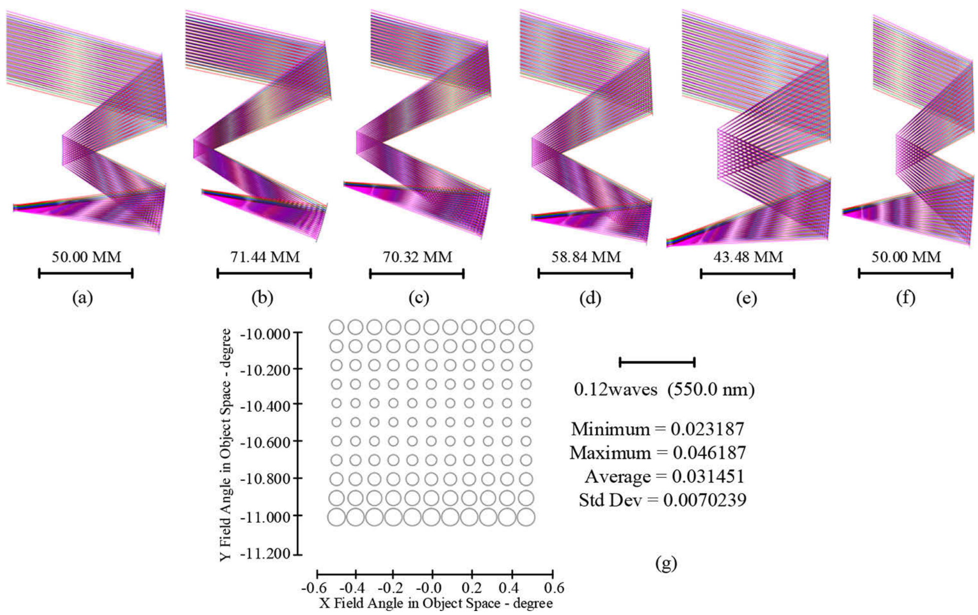

Fig. 12. Layout and RMS WFE. (a)System 0; (b)System 1; (c) System 7; (d) System 10; (e) System 11; (f) System 13; (g) "System 11" field map of the RMS WFE

4.3. Sensitivity analysis

We first analyze the S and the ΔRMS WFE when the system generates tilt errors (tilt error angle is 0.01°sagittal, 0.01° tangential) of "System 1", as shown in Fig. 13.

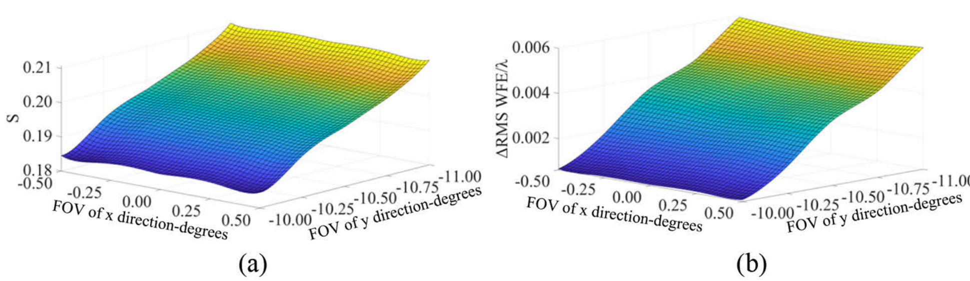

Fig. 13. The S of "System 1" and ΔRMSWFE diagram. (a)S, (b) ΔRMS WFE

Optics EXPRESS

Next, the S of each mirror in "System 1" and "System 11" and the ΔRMS WFE when the system generates tilt errors are analyzed in detail. The S of the *PM* and the ΔRMS WFE when generating the tilt are shown in Fig. 14(a), Fig. 14(b), while the S of the *SM* and the ΔRMS WFE when generating the tilt are shown in Fig. 14(c), Fig. 14(d), and the S of the *TM* and the ΔRMS WFE when generating the tilt are shown in Fig. 14(e), Fig. 14(f).

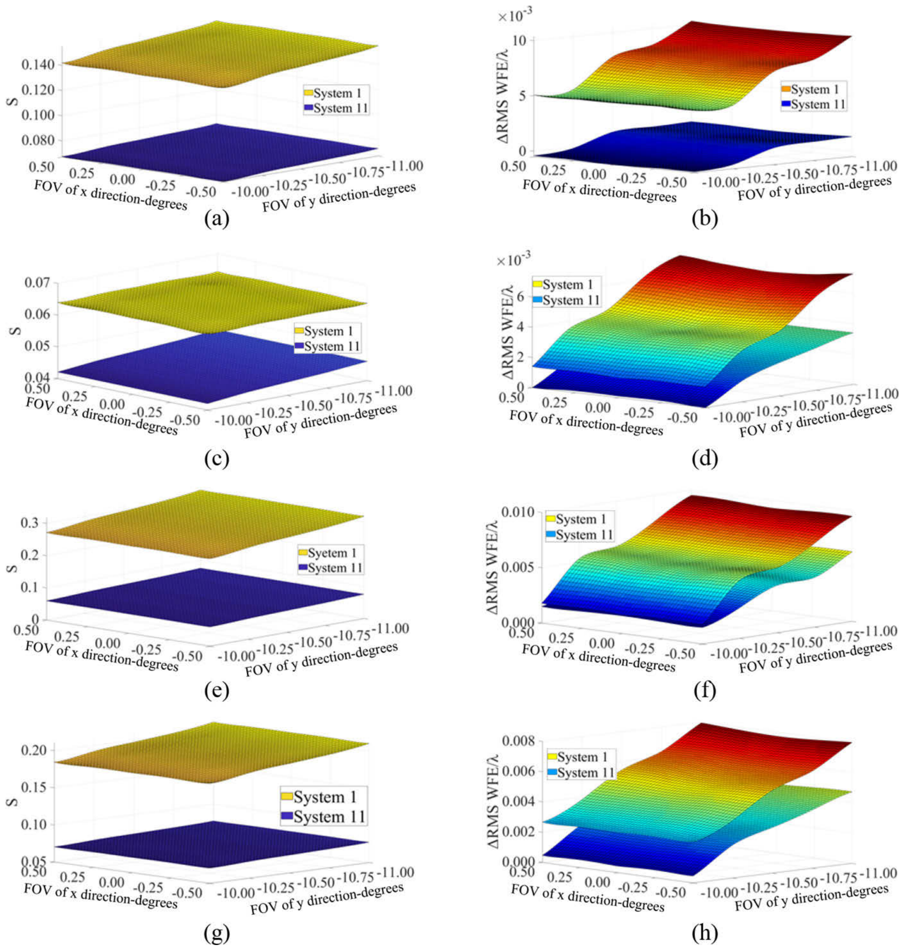

Fig. 14. S and ΔRMS WFE diagram. (a) PM-S comparison, (b) PM-ΔRMS WFE comparison, (c) SM-S comparison, (d) SM-ΔRMS WFE comparison, (e) TM-S comparison, (f) TM-ΔRMS WFE comparison; (g) S of system comparison (h) ΔRMS WFE of system comparison

The S comparison plots and ΔRMS WFE comparison plots for "System 1" (without using the proposed method) and "System 11" (using the proposed method) are shown in Fig. 14(g) and Fig. 14(h). After the analysis, the RMS WFE of "System 1" is 0.0297λ, and Sen=0.197 ± 0.1021, and the average ΔRMS WFE=0.0052λ when the tilt error is applied. The RMS WFE of "System 11" is 0.0314λ, and Sen=0.074 ± 0.0105, and the average ΔRMS WFE=0.0028λ when the tilt error is applied. With the same tilt error interruption, the ΔRMS WFE of the system that used the proposed method is 53.8% of that of the system without using the proposed method, which proves that the desensitization design method is correct and effective.

Optics EXPRESS

4.4. Large sample optimization and optimal threshold analysis

The judgement threshold of S is determined initially in Section 4.1. However, during the optimization process, we found that the S of "System 11" is 0.074 which is much smaller than 0.085, indicating that there is still a great potential for desensitization design for the 3000 systems. In order to determine the optimal threshold of S, we improved the evaluation standard of tilt error sensitivity and raised the threshold to 0.080. The proposed method was used to optimize the design of all 3000 systems. The distribution of their S is shown in Fig. 15, in which the blue points are the initial S and the red points are the S of the systems after desensitization. The comparison of the results shows that the S of the tilt error sensitivity of the system before optimization is distributed in the interval of (0.085, 0.120) with a mean value of 0.100, after desensitization optimization, and the S is distributed in the interval of (0.070, 0.083) with a mean value of 0.075, among which 2866 (95.53% of the overall) systems have the S less than 0.080. The error sensitivity performance of the 3000 optical systems has been improved overall.

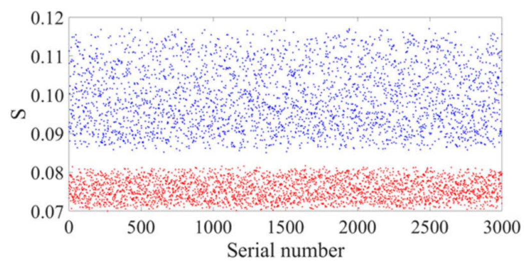

Fig. 15. S distribution of 3000 groups system

5. Conclusion

In order to obtain a reflective optical system with low tilt error sensitivity, this paper theoretically research the optical parameters which are relevant with the tilt error sensitivity. Based on geometric ray tracing method, derive the variation of OPD caused by the mirror tilt error, and the relationship between the slope of the tangent line at the intersection of the ray and the mirror and the error sensitivity is determined. A tilt error sensitivity evaluation function S is proposed, together with the evaluation function Sen that can comprehensively evaluate the uniformity of the error sensitivity distribution of each mirror in the optical system. Furthermore, a reflective optical system desensitization design method is established. To verify the theoretically research correctness and the desensitization design method effectiveness, an off-axis three-mirror optical system with a focal length of 100 mm, an F-number of 5, and an FOV of $1°\times1°$ is designed. By calculating and comparing the value of S and the ΔRMS WFE caused by the tilt error of each mirror and optical system before and after desensitization design, it shows that the S and the ΔRMS WFE caused by the error have the certain consistent positive correlation, which verify the correctness of the proposed error sensitivity evaluation function and the effectiveness of the desensitization design method.

Funding. National Natural Science Foundation of China (61705220); Youth Innovation Promotion Association of the Chinese Academy of Sciences (2019219); Strategic Priority Research Program of Chinese Academy of Sciences (XDA17010205).

Disclosures. The authors declare no conflicts of interest.

Data availability. Data underlying the results presented in this paper are not publicly available at this time but may be obtained from the authors upon reasonable request.

Optics EXPRESS

References

1. R. Gilmozzi and J. Spyromilio, "The European Extremely Large Telescope (E-ELT)," The Messenger **127**(11), 11–19 (2007).
2. G. Sanders, "The Thirty Meter Telescope (TMT): An International Observatory," J. Astrophys. Astron. **34**(2), 81–86 (2013).
3. M. Johns, P. McCarthy, K. Raybould, A. Bouchez, and M. Sheehan, "Giant magellan telescope: overview," Proc. SPIE **8444**, 84441H (2012).
4. D. Lindley, "Hubble Telescope has misshapen mirror," Nature **346**(5), 3 (1990).
5. P. Sabelhaus and J. Decker, "An overview of the james webb space telescope (JWST) project," Proc. SPIE **5899**, 58990P (2005).
6. Q. Meng, D. Wang, X. Wang, W. Li, X. Yang, D. Yan, Y. Li, Z. Cao, Q. Ji, T. Sun, W. Yan, K. Wang, X. Li, J. Huang, Z. Wang, W. Zhao, Y. Wang, Y. He, X. Hao, W. Liu, B. Zhang, P. Zhou, Y. Li, H. Zhao, L. Lu, H. Guan, D. Zhou, F. Wu, F. Zhang, S. Zhu, and J. Dong, "High Resolution Imaging Camera (HiRIC) on China's First Mars Exploration HX-1 Mission," Space Sci. Rev. **217**(3), 42 (2021).
7. T. Yang, J. Zhu, and G. Jin, "Design of free-form imaging systems with linear field-of-view using a construction and iteration process," Opt. Express **22**(3), 3362–3374 (2014).
8. J. Zhu, W. Hou, X. Zhang, and G. Jin, "Design of a low F-number free form off-axis three-mirror system with rectangular field-of-view," J. Opt. **17**(1), 015605 (2015).
9. X. Zhang, L. Zheng, X. He, L. Wang, F. Zhang, S. Yu, G. Shi, B. Zhang, Q. Liu, and T. Wang, "Design and fabrication of imaging optical systems with freeform surfaces," Proc. SPIE **8486**, 848607 (2012).
10. D. Li, W. Rao, C. Hu, Y. Wang, Z. Tang, and Y. Wang, "Overview of the Chinese space station manipulator," in *AIAA SPACE Conferences and Exposition (AIAA)* (2015), pp.4540–4545.
11. X. Zhang, J. Zhang, L. Wang, G. Shi, Y. Wu, L. Wang, F. Zeng, H. Qu, J. Zhang, H. Wu, Y. Zhu, and C. Wang, "Optical design of off-axis astronomical space telescope based on freeform surfaces," Proc. SPIE **9293**, 92930P (2014).
12. M. Postman, V. Argabright, B. Arnold, and B. Woodgate, "Advanced Technology Large-Aperture Space Telescope (ATLAST): A technology roadmap for the next decade," arXiv:0904.0941 (2009).
13. P. McGuire and James, "Designing Easily Manufactured Lenses Using a Global Method," Proc. SPIE **6342**, 63420O (2006).
14. Q. Meng, H. Wang, W. Wang, and Z. Yan, "Desensitization design method of unobscured three-mirror anastigmatic optical systems with an adjustment-optimization-evaluation process," Appl. Opt. **57**(6), 1472–1481 (2018).
15. M. Isshiki, L. Gardner, and G. Gregory, "Automated control of manufacturing sensitivity during optimization," Proc. SPIE **5249**, 343–352 (2003).
16. M. Isshiki, H. Ono, K. Hiraga, J. Ishikawa, and S. Nakadate, "Lens design: Global optimization with Escape Function," Opt. Rev. **2**(6), 463–470 (1995).
17. K. Fuse, "Method for designing a refractive or reflective optical system and method for designing a diffraction optical element," U.S. Patent 6567226 (20 May 2003).
18. L. Scaduto, J. Sasian, M. Stefani, and N. Jcdc, "Two-mirror telescope design with third-order coma insensitive to decenter misalignment," Opt. Express **21**(6), 6851–6865 (2013).
19. L. Wang and J. Sasian, "Merit figures for fast estimating tolerance sensitivity in lens systems," Proc. SPIE **7652**, 7652P (2010).
20. D. Grey, "Tolerance sensitivity and optimization," Appl. Opt. **9**(3), 523–526 (1970).
21. L. Chen, Z. Gao, J. Ye, X. Cao, N. Xu, and Q. Yuan, "Construction method through multiple off-axis parabolic surfaces expansion and mixing to design an easy-aligned freeform spectrometer," Opt. Express **27**(18), 25994–26013 (2019).
22. Q. Yuan, D. Zhu, and Z. Gao, "Alignment analyses of galvanometer based scanner in free space Fourier domain optical coherence tomography," Appl. Opt. **54**(32), 9554 (2015).
23. Q. Yuan, Z. Gao, and D. Zhu, "Applying slope constrained Qbfs aspheres for asphericity redistribution in the design of infrared transmission spheres," Appl. Opt. **54**(22), 6857 (2015).
24. T. Yang, D. Cheng, and Y. Wang, "Designing freeform imaging systems based on reinforcement learning," Opt. Express **28**(20), 30309–30323 (2020).
25. T. Yang, G. Jin, and J. Zhu, "Automated design of freeform imaging systems," Light: Sci. Appl. **6**(10), e17081 (2017).
26. B. Ma, K. Sharma, K. Thompson, and J. Rolland, "Mobile device camera design with Q-type polynomials to achieve higher production yield," Opt. Express **21**(15), 17454–17463 (2013).
27. J. Bentley, S. Stoebenau, K. Thompson, and J. Rolland, "Why are freeform telescopes less alignment sensitive than a traditional unobscured TMA?" Proc. SPIE **9633**, 963317 (2015).
28. Y. Zhong, H. Gross, A. Broemel, S. Kirschstein, P. Petruck, and A. Tuennermann, "Investigation of TMA systems with different freeform surfaces," Proc. SPIE **9626**, 96260X (2015).
29. X. Liu, T. Gong, G. Jin, and J. Zhu, "Design method for assembly-insensitive freeform reflective optical systems," Opt. Express **26**(21), 27798–27811 (2018).